NASA Technical Memorandum 108815

Direct Simulation of a Self-Similar Plane Wake

Robert D. Moser and Michael M. Rogers

April 1994

National Aeronautics and Space Administration

NASA Technical Memorandum 108815

Direct Simulation of a Self-Similar Plane Wake

Robert D. Moser and Michael M. Rogers, Ames Research Center, Moffett Field, California

April 1994

National Aeronautics and
Space Administration

Ames Research Center
Moffett Field, California 94035-1000

Direct Simulation of a Self-Similar Plane Wake

Robert D. Moser and Michael M. Rogers

NASA Ames Research Center
Moffett Field CA, 94035
USA

1. SUMMARY

Direct simulations of two time-developing turbulent wakes have been performed. Initial conditions for the simulations were obtained from two realizations of a direct simulation of a turbulent boundary layer at momentum thickness Reynolds number 670. In addition, extra two-dimensional disturbances were added in one of the cases to mimic two-dimensional forcing. The unforced wake is allowed to evolve long enough to attain self-similarity. The mass-flux Reynolds number (equivalent to the momentum thickness Reynolds number in spatially developing wakes) is 2000, which is high enough for a short $k^{-5/3}$ range to be evident in the streamwise one-dimensional velocity spectrum.

Several turbulence statistics have been computed by averaging in space and over the self-similar period in time. The growth rate in the unforced flow is low compared to experiments, but when this growth-rate difference is accounted for, the statistics of the unforced case are in reasonable agreement with experiments. However, the forced case is significantly different. The growth rate, turbulence Reynolds number, and turbulence intensities are as much as ten times larger in the forced case. In addition, the forced flow exhibits large-scale structures similar to those observed in transitional wakes, while the unforced flow does not.

2. INTRODUCTION

The plane wake studied here is one of several canonical free shear flows that are used as test flows for the development of turbulence models and turbulence control strategies. In addition, plane wakes are of particular interest in high-lift airfoil configurations, where one lifting surface (a flap) may be operating in or near the wake of an upstream surface. The numerical simulations reported here are the first of several to be performed to provide data for turbulence modeling relevant to such a configuration.

It is well known that a turbulent plane wake will approach a self-similar evolution, with thickness growing like $x^{1/2}$, where x is streamwise distance. However, the rate at which this growth occurs can vary considerably. For example, in the experiments of Wygnanski *et al.*,[1] the growth rate $\frac{1}{\theta}\frac{db^2}{dx}$ (b is the half-width of the wake, defined below, and θ is the momentum thickness) varied from 0.29 to 0.41 depending on the details of the body that generated the wake. Even larger growth rates can be obtained using two-dimensional forcing.[1,2] Furthermore, as pointed out by George[3] and as observed by Wygnanski *et al.*,[1] even if the mean velocity profiles of various plane wakes are the same (when properly scaled), profiles of the turbulence statistics need not be.

As in many free-shear flows, the evolution of large-scale coherent structures in the plane wake has been of great interest (*e.g.* Refs. 4 and 5). Part of the reason for this interest is that the well-known features of transitional wakes (*e.g.* the Karman street) have been observed in the turbulent wake as well. However, the extent to which such structures are dynamically important, and how they might vary among different wakes is not clear.

The apparent non-uniqueness of the self-similar plane wake is a problem because it complicates the modeling of the flow. At the same time, it provides an opportunity to control the evolution of the wake. Progress in predicting and/or controlling the wake evolution will be facilitated by more detailed information on both the statistics and structures in plane wakes, how they are related, and how and why they vary among different wakes. Direct numerical simulation is an ideal tool for providing some of this information because it provides absolute control of the initial/inlet conditions and very detailed information about the flow. Two such simulations with differing initial conditions were performed to address these issues, and some of the preliminary results are reported here. The simulations are described in §3, a statistical description of the two flows is presented in §4, and the structural features of the flows are discussed in §5. Finally, some concluding remarks are given in §6.

3. THE SIMULATIONS

The numerical simulations discussed in this paper were performed by solving the three-dimensional time-dependent incompressible Navier–Stokes equations. For computational efficiency, a temporally evolving plane wake was simulated rather than the spatially evolving

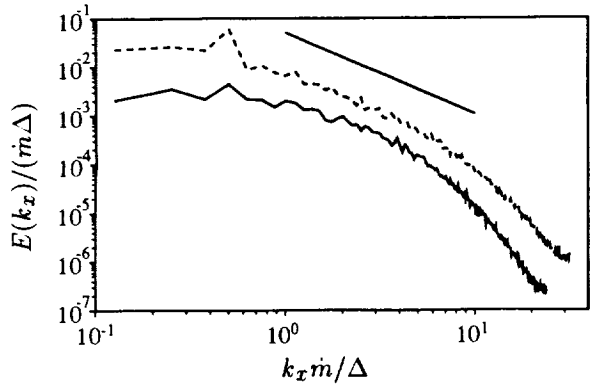

Figure 1. Streamwise one-dimensional energy spectra at $y = 0$ in the —— unforced wake simulation at $t\Delta^2/\dot{m} = 91.5$ and ---- the forced wake simulation at $t\Delta^2/\dot{m} = 50.0$. The straight line shows a $k^{-5/3}$ dependence.

flow typical of experiments. The spatially and temporally evolving wakes differ in that different integral quantities are preserved. In the time-developing wake, the cross-stream integrated mass flux deficit $\dot{m} = -\int_{-\infty}^{\infty} \delta U \, dy$ is preserved (the velocity deficit is $\delta U = \overline{U} - U_\infty$, where $\overline{U}$ and U_∞ are the mean and free-stream velocities, respectively), while in the spatially evolving wake, the integrated momentum flux deficit $U_\infty^2\theta = -\int_{-\infty}^{\infty} \delta U(U_\infty + \delta U)\, dy$ is preserved. In the limit of small deficits, the temporally evolving wake is equivalent to a spatially evolving wake viewed in a frame moving with the free stream, and in this limit, the mass flux deficit is given by $\dot{m} = U_\infty\theta$. In the time-developing wake, the free stream velocity is irrelevant, only the deficit is important. Thus, in what follows, nondimensionalization will be based on $\dot{m}$ and the initial magnitude of the velocity deficit, Δ. In both flows described here, the Reynolds number $Re_m = \dot{m}/\nu$ is 2000. This Reynolds number is high enough to produce a short $k^{-5/3}$ spectral range in the streamwise one-dimensional spectrum (figure 1).

In this study, the solution domain is periodic in the streamwise (x) and spanwise (z) directions with periods $50\dot{m}/\Delta$ and $12.5\dot{m}/\Delta$ respectively. These domain sizes were selected to correspond to those in the boundary layer simulations from which the initial conditions were obtained (see below). The domain is infinite in the cross-stream (y) direction. A Galerkin spectral method[6] was used to solve the equations.

Initial conditions were generated using two realizations of a turbulent boundary layer with a momentum thickness Reynolds number of 670, as computed by Spalart[7]. One boundary layer was used for each side of the wake, with equal free stream velocities attained at $y = \pm\infty$. Thus, the simulations represent a temporally evolving approximation to the wake of a zero-thickness flat plate with turbulent boundary layers at zero angle of attack. In addition to the boundary layers and their turbulence, one of the two simulations included extra two-dimensional forcing in the initial condition. This forcing was used to mimic the expected receptivity of the trailing edge of the plate to two-dimensional disturbances. To model the uncontrolled nature of the two-dimensional disturbances in a flat-plate wake, the forcing was introduced by amplifying all the two-dimensional modes in the boundary layer initial conditions by a factor of 20. In similar simulations in a mixing layer,[8] this amplification factor was needed to produce a significant effect. The amplification increased the total initial disturbance energy by a factor of 13, and the total energy per unit plan area added to the flow by the forcing was $0.7\dot{m}\Delta$.

4. SELF-SIMILARITY AND STATISTICS

Developed small deficit plane wakes evolve self-similarly, with thicknesses growing like $t^{1/2}$ (or $x^{1/2}$ in a spatially developing wake). Since in a time-evolving wake the total mass flux deficit $\dot{m}$ is constant, this implies that the maximum velocity deficit magnitude (U_0) decays like $t^{-1/2}$. In a spatially evolving wake, the momentum thickness θ is constant, which implies that a $x^{-1/2}$ decay of the deficit holds in this case. By scaling large-scale quantities with the local thickness and the velocity deficit, statistical profiles at different times (or different downstream locations in the spatially evolving flow) collapse onto a single curve. In what follows, the numerically simulated plane wake is examined for evidence of such self-similar evolution.

A variety of different thickness measures can be used to characterize the wake locally. To facilitate comparison to previous experimental data, we will use the half-width b, which is defined to be the distance between the y-locations at which the mean velocity is half of U_0 (note that some investigators take the half-width to be half this distance).

Shown in figure 2 are the time evolutions of b^2 and U_0^{-2} for the unforced and forced cases. Both these quantities should evolve linearly during self-similarity, and indeed in the unforced flow both have substantial periods of linear growth. The normalized growth rate (α) is

$$\alpha = \frac{1}{\dot{m}}\frac{db^2}{dt} = \frac{d(b\Delta/\dot{m})^2}{d\tau}, \qquad (1)$$

where the nondimensional time τ is given by $\tau = t\Delta^2/\dot{m}$. In the unforced flow $\alpha = 0.23$, which is significantly smaller than the experimental value of 0.34 in Ref. 9. In contrast, the forced case has no extended period of self-similar growth, though there are short periods during which b^2 and/or U_0^{-2} develop linearly. The best chance for self-similarity in the forced case occurs near the end of the simulation ($\tau > 40$). Here bU_0 (figure 2(c)) appears to be reaching a plateau indicating that b and U_0 are evolving together ($\alpha = 1.63$ at this time in the unforced flow). Furthermore the statistical profiles discussed below are roughly consistent with self-similarity.

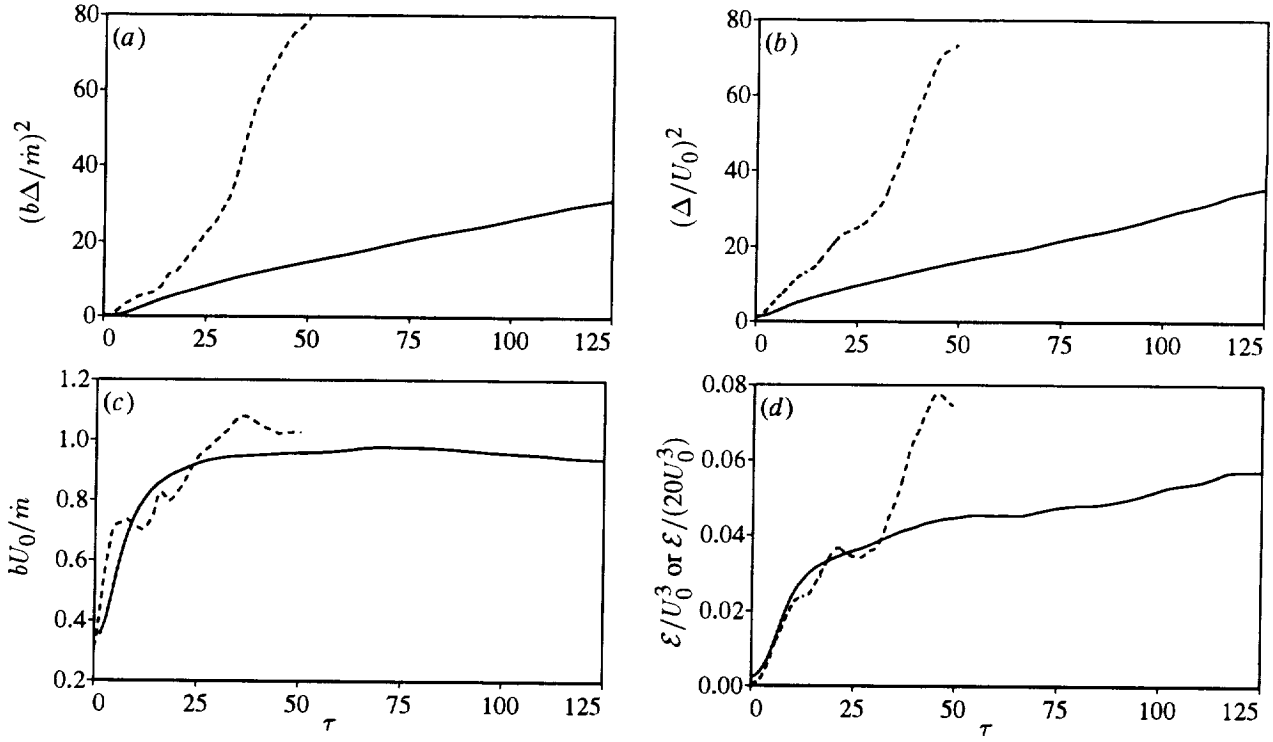

Figure 2. Evolution of (*a*) $(b\Delta/\dot{m})^2$, (*b*) $(\Delta/U_0)^2$, (*c*) $bU_0/\dot{m}$, and (*d*) $\mathcal{E}/U_0^3$ or $\mathcal{E}/(20U_0^3)$ in the —— unforced and ---- forced wake simulations, respectively.

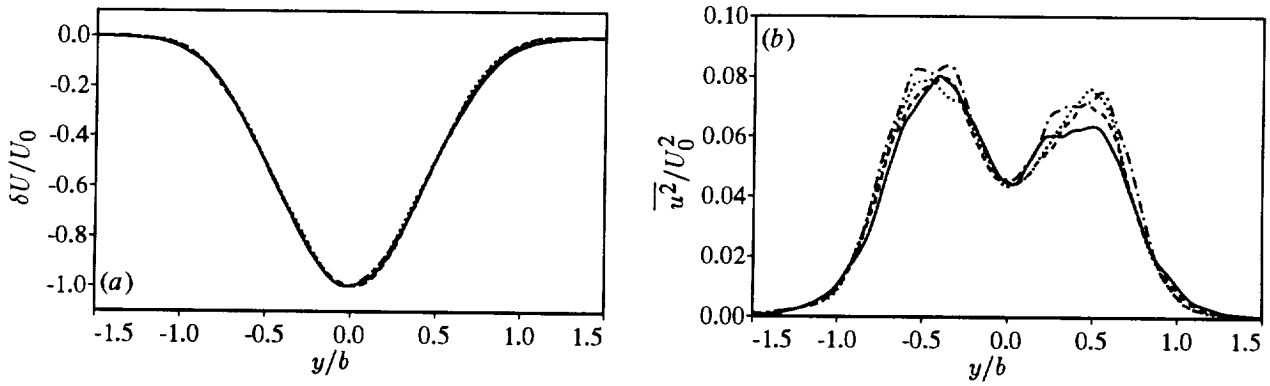

Figure 3. Collapse of (*a*) $\delta U/U_0$ and (*b*) $\overline{u^2}/U_0^2$ in scaled coordinates at four times during the self-similar period at —— $\tau = 42.8$, ---- $\tau = 56.6$, ····· $\tau = 71.7$ and —·— $\tau = 91.5$.

Another global quantity that can be examined for evidence of self-similarity is

$$\mathcal{E} = \int_{-\infty}^{\infty} \epsilon \, dy \,, \tag{2}$$

the integrated rate of dissipation of kinetic energy ($\epsilon = 2\nu\overline{S_{ij}S_{ij}}$, where S_{ij} is the strain-rate tensor and ν is the kinematic viscosity). This quantity has units of velocity cubed and therefore should scale with U_0^3. Thus $\mathcal{E}/U_0^3$ should be a constant during self-similarity. In figure 2(*d*), it is shown that $\mathcal{E}/U_0^3$ is indeed approximately constant for $40 \leq \tau \leq 90$ in the unforced case, but the evidence for self-similarity is less convincing during the approximately self-similar period ($\tau > 40$) in the forced case.

The self-similarity of the unforced flow is further supported by the mean velocity and Reynolds stress profiles, when plotted in self-similar coordinates. Shown in figure 3 are the mean velocity and streamwise velocity variance at four times in the self-similar period ($42.8 \leq \tau \leq 91.5$) of the unforced flow. The collapse of these curves is good. Profiles from times outside of this period (not shown) do not collapse nearly as well. As in the mixing layer simulations in Ref. 8, the breakdown of self-similarity at late times appears to be caused by the finite size of the computational domain. In the forced flow, the mean and variance profiles also collapse quite well during the approximate self-similar period ($\tau > 40$).

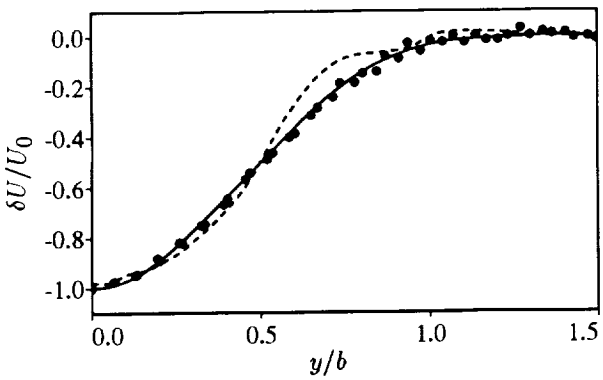

Figure 4. Comparison of time-averaged (in scaled coordinates) wake deficit profiles from ——— , the unforced wake simulation, ---- the forced wake simulation, and • the experiments of Ref. 9.

Since the average quantities collapse in self-similar coordinates, they can also be averaged in time over the self-similar period, reducing the statistical noise in the profiles. The results of such averaging are shown in figures 4 and 5 for the mean velocity and Reynolds stress components, respectively. Also shown are the data from Ref. 9. Note that the magnitudes of the Reynolds stress components in the forced case are an order of magnitude larger than the curves shown in figure 5, and are therefore omitted (see figure 6). Since the wake is statistically symmetric, the statistical sample in these profiles has been increased by averaging the two sides of the wake together. Only half of each average profile is shown. The agreement between the experimental and unforced computational mean velocity is very good. However, the mean profile from the forced flow does not agree as well, and is not smooth. This is presumably because of the poor statistical sample of the large structures that dominate the forced flow (see §5). The components of the Reynolds stress tensor in the unforced computation shown in figure 5 have the same general shape as those measured in the Weygandt & Mehta[9] experiments, but the magnitudes are smaller.

Part of the reason for this difference in Reynolds stress magnitude is the difference in growth rates noted above. As was pointed out by George,[3] a variety of self-similar turbulent flows could occur in the same flow situation, and even if the (normalized) mean velocities are the same, the growth rates, Reynolds stresses, and dissipation rates (for example) can differ. In fact there is a direct relationship between the magnitude of the (normalized) Reynolds shear stress and the growth rate α. To see this, express the mean velocity and Reynolds shear stress in self-similar form:

$$\delta U = U_0 f(\zeta) \qquad -\overline{uv} = Rg(\zeta), \tag{3}$$

where $\zeta = y/b$, f and g are the self-similar profiles, and R is the scale for the Reynolds stress. In the time-developing wake, the mean velocity equation (in the inviscid limit) is

$$\frac{\partial \delta U}{\partial t} = -\frac{\partial \overline{uv}}{\partial y} . \tag{4}$$

Substituting the self-similar forms, evaluating the derivatives, and rearranging yields

$$f + \zeta f' = -\frac{2bR}{\dot{m}\alpha U_0} g' . \tag{5}$$

If two different wakes have the same f, then they must have the same g' profile and the scaling R must be given by

$$R = U_0^2 \alpha \frac{\dot{m}}{U_0 b} . \tag{6}$$

Since $\dot{m}/(U_0 b)$ is a shape factor of order one (see figure 2(c)), the Reynolds shear stress should scale like $U_0^2\alpha$. It is reasonable to assume that all components of the Reynolds stress tensor scale this way, and that at least some of the differences in the velocity variances shown in figure 5 are due to growth rate differences.

Profiles of the Reynolds stress tensor components normalized by $U_0^2\alpha$ are shown in figure 6 for both the simulations and the experiments of Ref. 9. This scaling with α has indeed reduced the differences among the different wakes. The unforced simulation and the experiments agree well with regard to the level of $\overline{u^2}$, $\overline{w^2}$, and $\overline{uv}$, but the level of $\overline{v^2}$ is still about 30% higher in the experiments. It is interesting that the levels of $\overline{u^2}$ and $\overline{v^2}$ in the forced case can be several times larger than those in the other data, while the $\overline{w^2}$ and $\overline{uv}$ profiles agree reasonably well for all three wakes when scaled with $U_0^2\alpha$. Apparently the strong forcing of the two-dimensional modes has produced a wake that is qualitatively different from the other two wakes (see §5). As pointed out in Ref. 3, the profiles of all the Reynolds stress tensor components are not expected to collapse perfectly in this scaling due to the unknown variation of the various terms in the Reynolds stress balance equations. A similar variation in the shapes of the $\overline{u^2}$ profiles in different wakes was reported in Ref. 1.

In addition to velocity statistics, vorticity statistics can be obtained from the simulations. As in Ref. 8, the scaling of $\mathcal{E}$ with U_0^3 implies that the vorticity variances should scale like $Re_b U_0^2/b^2$, where $Re_b = U_0 b/\nu$. However, since Re_b is a constant in a self-similar wake, the Reynolds number factor would only be important when comparing wakes at different Reynolds numbers. The vorticity variances averaged over the self-similar period in the unforced flow are shown in figure 7. The relative magnitudes of the variances of the vorticity components are in general agreement with those found in previous computations of homogeneous shear flows[10] and plane mixing layers[8].

Some of the more difficult statistical quantities to determine experimentally are the terms in the balance equations for the Reynolds stresses. As an example, consider

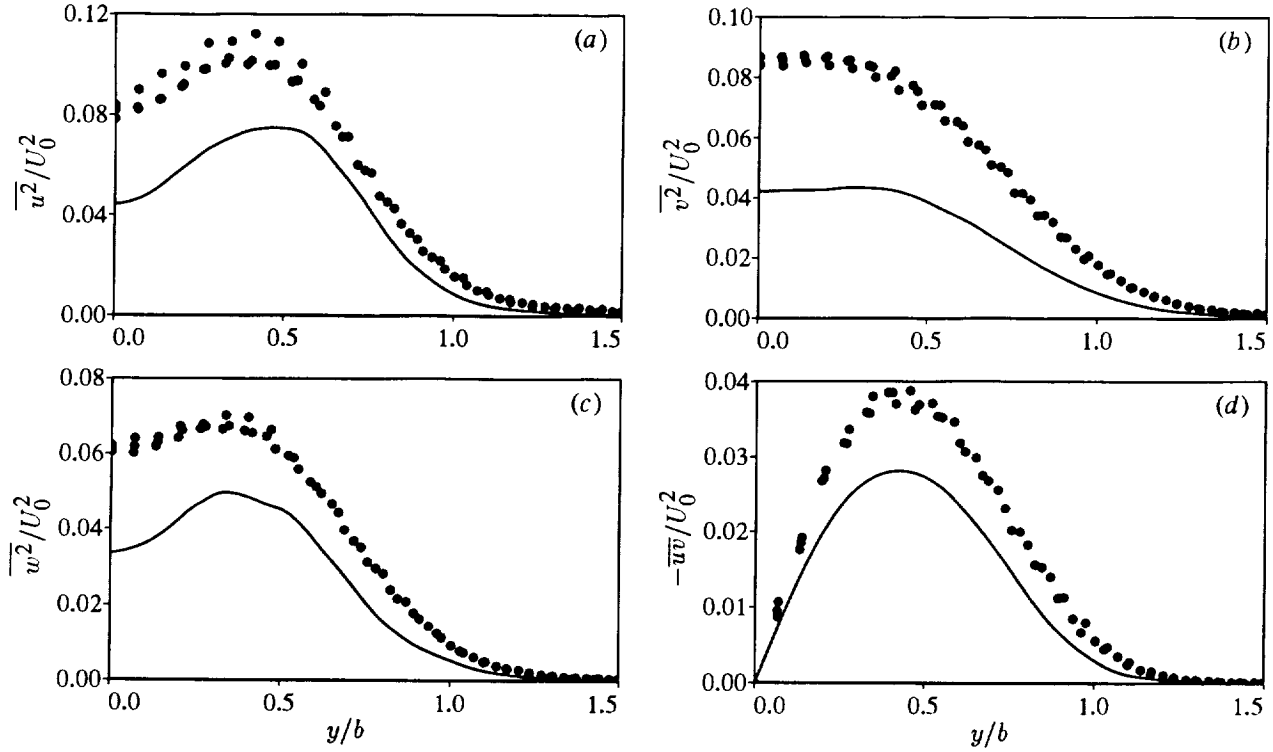

Figure 5. Comparison of the time-averaged (in scaled coordinates) components of the Reynolds stress tensor from ——— , the unforced simulations, and • the experiments of Ref. 9.

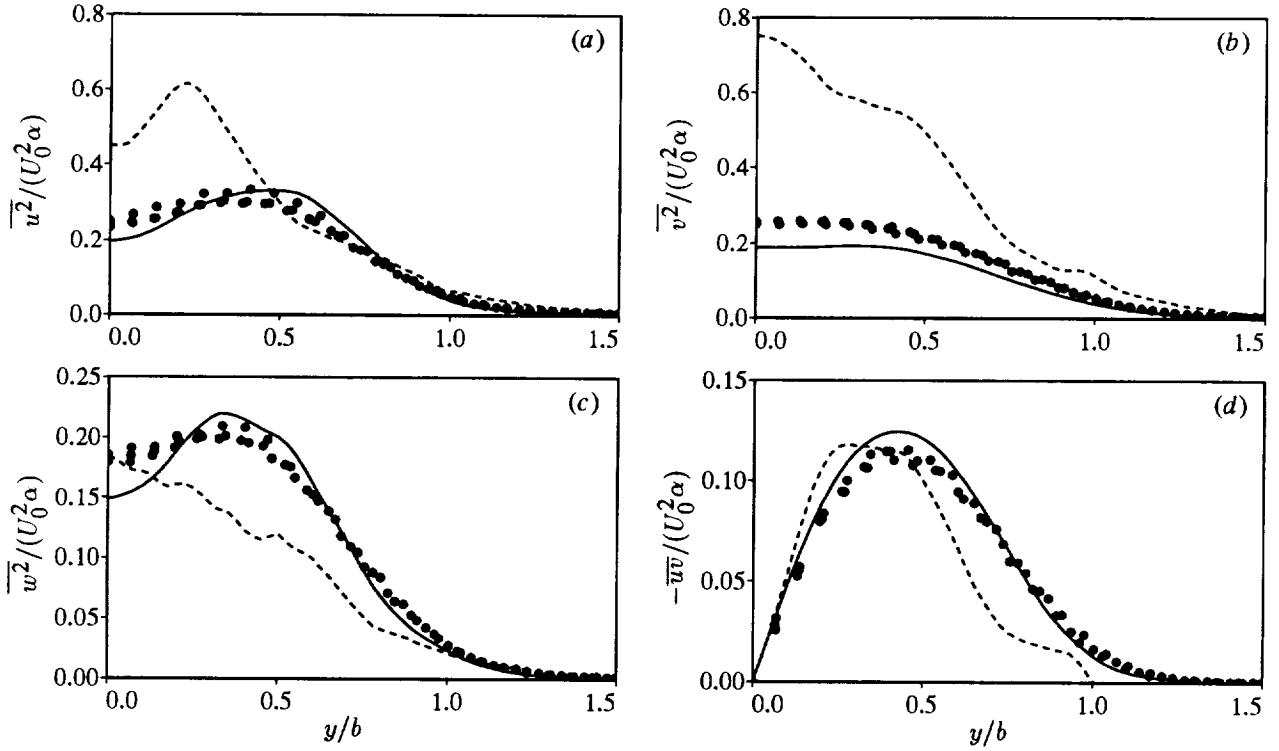

Figure 6. Comparison of the time-averaged (in scaled coordinates) profiles of $\overline{u^2}$, $\overline{v^2}$, $\overline{w^2}$, and $\overline{uv}$ normalized by $U_0^2\alpha$ from ——— , the unforced wake simulation, - - - - the forced wake simulation, and • the experiments of Ref. 9.

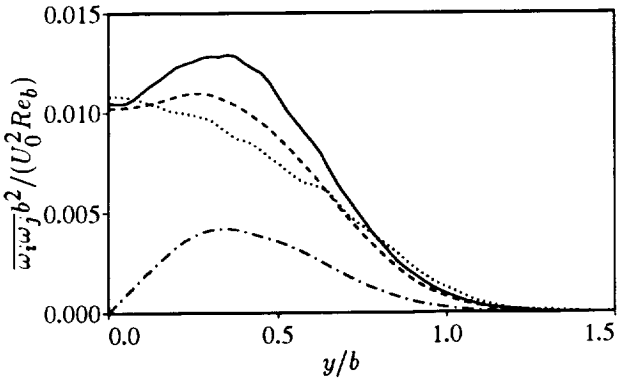

Figure 7. Time-averaged (in scaled coordinates) vorticity correlation tensor profiles $\overline{\omega_i\omega_j}$. —— $\overline{\omega_1^2}$, ---- $\overline{\omega_2^2}$, ····· $\overline{\omega_3^2}$, —·— $\overline{\omega_1\omega_2}$.

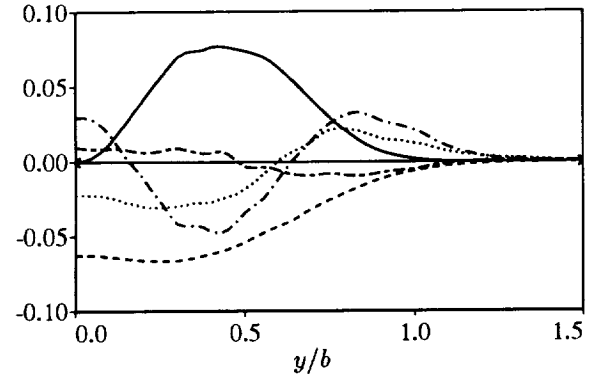

Figure 8. Terms in the $\overline{q^2}$ balance equation, scaled by U_0^3/b. —— production ---- dissipation ····· time derivative, —·— turbulent diffusion, and —— pressure diffusion.

the equation for $\overline{q^2} = \overline{u_i u_i}$, which in this case of the time-developing wake is given by

$$\frac{\partial \overline{q^2}}{\partial t} = -2\overline{uv}\frac{\partial \delta U}{\partial y} - \frac{\partial \overline{q^2 v}}{\partial y} - \frac{\partial \overline{pv}}{\partial y} - \frac{2}{Re}\overline{\frac{\partial u_i}{\partial x_j}\frac{\partial u_i}{\partial x_j}} + \frac{1}{Re}\frac{\partial^2 \overline{q^2}}{\partial y^2} \tag{7}$$

The terms on the right hand side are interpreted (in order of appearance) as production, turbulent diffusion, pressure diffusion, dissipation, and viscous diffusion. The average of the terms in this equation over the self-similar period in the unforced flow are shown in figure 8.

Since the shear is zero at the center of the wake, the production is zero there. Production of $\overline{q^2}$ thus peaks in the maximum shear region and turbulent diffusion provides transport to the center of the wake. Turbulent diffusion also transports $\overline{q^2}$ to the edge of the wake, and is thus responsible for most of the growth in the width of the $\overline{q^2}$ profile. There is also a small transport from the edge of the wake to the center by pressure diffusion. The negative time derivative near the center of the wake produces the t^{-1} decay in the maximum $\overline{q^2}$, and the growth in the width of the turbulent region is reflected in the positive time derivative at the edge of the wake. For a self-similar wake, the time derivative can be computed directly from the $\overline{q^2} = U_0^2 h(\zeta)$ profile, with the result

$$\frac{b}{U_0^3}\frac{\partial \overline{q^2}}{\partial t} = -\frac{\dot{m}}{U_0 b}\alpha\left(h + \frac{1}{2}\zeta h'\right) . \tag{8}$$

At the centerline, $h = \overline{q^2}/U_0^2$ is 0.12 and the shape factor $\dot{m}/(U_0 b)$ is 1.04 (see figure 2(c)), resulting in a centerline value of the time derivative of 0.028. This is somewhat larger than the value (0.023) computed from the simulation data and plotted in figure 8. The discrepancy is a measure of the departure of the unforced simulation from self-similarity, and the adequacy of the statistical sample.

5. STRUCTURES

The large statistical differences between the forced and unforced wakes discussed in §4 are a manifestation of differences in the structure of the turbulence in these two flows. This difference can be seen in figure 9, where spanwise vorticity contours in x–y planes of both the forced and unforced flows are shown. In the forced case, there are concentrations of vorticity fluctuations that occur alternately on one side of the wake or the other, similar to the Karman street commonly observed in transitional wakes. By examining other x–y planes (not shown), one can determine that these large-scale features are spanwise coherent. The vorticity concentrations are also accompanied by large incursions of irrotational fluid into the wake. In contrast, the unforced wake exhibits no such vorticity concentrations, and relatively small incursions of irrotational fluid. It appears to consist of a slab of turbulence with undulating boundaries. Forcing was also found to produce large-scale structures similar to those in transitional flows in the turbulent mixing layers of Ref. 8.

Another striking difference between the two flows is that the forced flow appears to have vorticity fluctuations of much smaller scale. This is consistent with the appearance of the streamwise spatial spectra in figure 1 and the fact that finer spatial resolution was required to compute the forced flow. Comparing figure 9(a) and figure 9(b), it appears that the forced flow has a larger Reynolds number than the unforced flow since there are larger large-scale features, and smaller small-scale features. Indeed the centerline value of the turbulence Reynolds number $q^4/(\epsilon\nu)$ is an order of magnitude larger in the forced case than in the unforced case (4000 versus 460), this despite the fact that the Reynolds numbers based on $\dot{m}$ are the same in the two flows.

The mixing layer simulations of Rogers & Moser[8,11] suggest that whenever there is a flow region that is dominated by large-scale strain, but largely devoid of (spanwise) vorticity, it is likely that long coherent vortices aligned with the extensional strain (so-called rib vortices), will

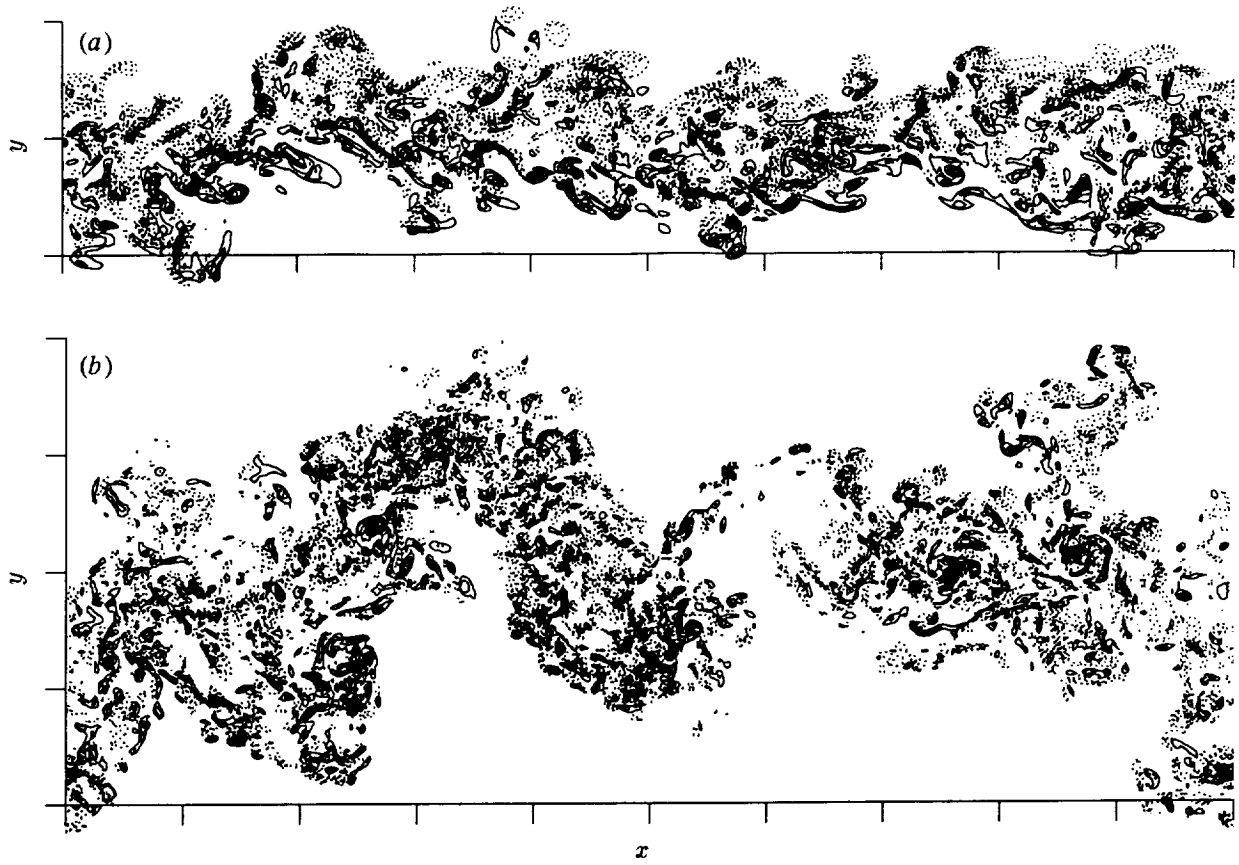

Figure 9. Contours of spanwise vorticity in an x–y plane in (a) the unforced flow at $\tau = 91.5$ and (b) the forced flow at $\tau = 50.0$. The contour increments are (a) $2.5U_0/b$ and (b) $20U_0/b$, and negative contours are dotted. Tic marks are at $5\dot{m}/\Delta$ intervals.

develop. Such a region might be expected between the vortices in a Karman Street, and indeed rib vortices have been observed in simulations of transitional wakes.[12] A strain-dominated region of this type appears to exist in the forced flow shown in figure 9(b)(at $x \approx 35\dot{m}/\Delta$), but no rib vortices were found at this time. However, at an earlier time ($\tau = 26.3$, figure 10), the strain-dominated region is also present and rib vortices occur there. The rib vortices can be seen in figure 10(b) as the long thin streamwise-oriented regions of large enstrophy at $x \approx 35\dot{m}/\Delta$. These vortices span the strain-dominated region, and do not occur elsewhere in the forced flow or anywhere in the unforced flow, which has no such strain-dominated regions. The reason for the disappearance of the rib vortices at later times has not yet been investigated.

6. CONCLUSIONS

Two turbulent time-developing plane wakes (forced and unforced) have been simulated numerically, and at least the unforced wake evolves self-similarly for a significant period. The growth rate of the unforced wake is low by 30% compared to experimentally observed growth rates. In the unforced flow, the magnitude of all the components of the Reynolds stress tensor except $\overline{v^2}$ are in general agreement with the experimental data of Ref. 9 when scaled by the growth rate. The vertical velocity variance is lower than the experiments by 30%.

The forced flow is not convincingly self-similar. But, toward the end of the simulation, it appears to be beginning a self-similar growth period. However, the growth rate α is an order of magnitude larger than in the unforced flow, and the turbulence levels are several times larger, even when the difference in growth rates is accounted for. Also, the turbulence Reynolds number is much larger than in the unforced flow, even though the bulk Reynolds numbers are the same. Finally, the forced flow exhibits large-scale structures similar to those observed in transitional wakes, though no such structures were present in the unforced flow. The strong forcing has resulted in a qualitatively different turbulent flow. It is not clear if this difference would be maintained if the flow could continue to evolve.

REFERENCES

1. I. Wygnanski, F. Champagne, and B. Marasli, "On the Large-scale Structures in Two-dimensional Small-deficit, Turbulent Wakes," J. Fluid Mech. **168**, 31 (1986).

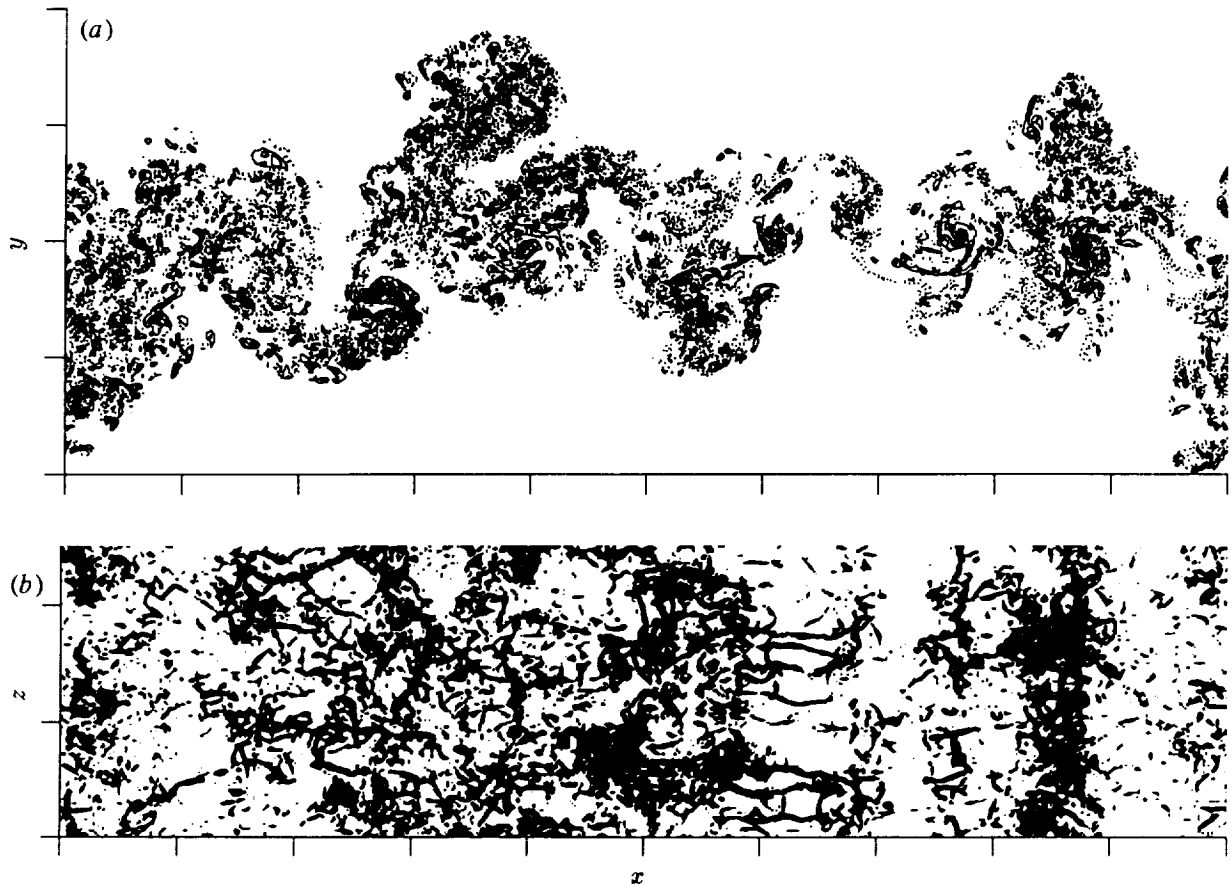

Figure 10. (a) Contours of spanwise vorticity in an x–y plane (contour increment of $10U_0/b$) and (b) top view of regions where enstrophy ($\omega_i\omega_i$) is larger than $8700U_0^2/b^2$ in the forced flow at $\tau = 26.3$. Tic marks are at $5\Delta/\dot{m}$ intervals.

2. B. Marasli, F. H. Champagne, and I. Wygnanski, "Effect of Travelling Waves on the Growth of a Plane Turbulent Wake," J. Fluid Mech. **235**, 511 (1992).

3. W. K. George, "The Self-Preservation of Turbulent Flows and its Relation to Initial Conditions and Coherent Structure," in *Advances in Turbulence*, edited by W. K. George and R. Arndt (Hemisphere, New York, 1989), pp. 39–73.

4. R. A. Antonia, L. W. B. Browne, and D. K. Bisset, "A Description fo the Organized Motion in the Turbulent Far Wake of a Cylinder at Low Reynolds Number," J. Fluid Mech. **184**, 423 (1987).

5. M. Hayakawa and F. Hussain, "Three-Dimensionality of Organized Structures in a Plane Wake," J. Fluid Mech. **206**, 375 (1989).

6. P. R. Spalart, R. D. Moser, and M. M. Rogers, "Spectral methods for the Navier–Stokes equations with one infinite and two periodic directions," J. Comp. Phys. **96**, 297 (1991).

7. P. R. Spalart, "Direct simulation of a turbulent boundary layer up to $R_\theta = 1410$," J. Fluid Mech. **187**, 61 (1988).

8. M. M. Rogers and R. D. Moser, "Direct Simulation of a Self-similar Turbulent Mixing Layer," Phys. Fluids **6**, 903 (1994).

9. J. H. Weygandt and R. D. Mehta, JIAA TR-110, Stanford University (1993).

10. M. M. Rogers and P. Moin, "The structure of the vorticity field in homogeneous turbulent flows," J. Fluid Mech. **176**, 33 (1987).

11. M. M. Rogers and R. D. Moser, "The three-dimensional evolution of a plane mixing layer: the Kelvin-Helmholtz rollup," J. Fluid. Mech. **243**, 183 (1993).

12. J. C. Lasheras and E. Meiburg, "Three-Dimensional Vorticity Modes in the Wake of a Flat Plate," Phys. of Fluids **2**, 371 (1990).

REPORT DOCUMENTATION PAGE

Form Approved
OMB No. 0704-0188

1. AGENCY USE ONLY *(Leave blank)*	2. REPORT DATE	3. REPORT TYPE AND DATES COVERED
	April 1994	Technical Memorandum

4. TITLE AND SUBTITLE

Direct Simulation of a Self-Similar Plane Wake

5. FUNDING NUMBERS

505-59-50

6. AUTHOR(S)

Robert D. Moser and Michael M. Rogers

7. PERFORMING ORGANIZATION NAME(S) AND ADDRESS(ES)

Ames Research Center
Moffett Field, CA 94035-1000

8. PERFORMING ORGANIZATION REPORT NUMBER

A-94070

9. SPONSORING/MONITORING AGENCY NAME(S) AND ADDRESS(ES)

National Aeronautics and Space Administration
Washington, DC 20546-0001

10. SPONSORING/MONITORING AGENCY REPORT NUMBER

NASA TM-108815

11. SUPPLEMENTARY NOTES

Point of Contact: Robert D. Moser, Ames Research Center, MS 202A-1, Moffett Field, CA 94035-1000; (415) 604-4733

12a. DISTRIBUTION/AVAILABILITY STATEMENT

Unclassified — Unlimited
Subject Category 34

12b. DISTRIBUTION CODE

13. ABSTRACT *(Maximum 200 words)*

Direct simulations of two time-developing turbulent wakes have been performed. Initial conditions for the simulations were obtained from two realizations of a direct simulation of a turbulent boundary layer at momentum thickness Reynolds number 670. In addition, extra two-dimensional disturbances were added in one of the cases to mimic two-dimensional forcing. The unforced wake is allowed to evolve long enough to attain self-similarity. The mass-flux Reynolds number (equivalent to the momentum thickness Reynolds number in spatially developing wakes) is 2000, which is high enough for a short $k^{-5/3}$ range to be evident in the streamwise one-dimensional velocity spectrum.

Several turbulence statistics have been computed by averaging in space and over the self-similar period in time. The growth rate in the unforced flow is low compared to experiments, but when this growth-rate difference is accounted for, the statistics of the unforced case are in reasonable agreement with experiments. However, the forced case is significantly different. The growth rate, turbulence Reynolds number, and turbulence intensities are as much as ten times larger in the forced case. In addition, the forced flow exhibits large-scale structures similar to those observed in transitional wakes, while the unforced flow does not.

14. SUBJECT TERMS	15. NUMBER OF PAGES
Turbulence, Wakes, Self-similarity, Direct simulation	12
	16. PRICE CODE: A03

17. SECURITY CLASSIFICATION OF REPORT	18. SECURITY CLASSIFICATION OF THIS PAGE	19. SECURITY CLASSIFICATION OF ABSTRACT	20. LIMITATION OF ABSTRACT
Unclassified	Unclassified		